

Collision-Free Trajectory Optimization in Cluttered Environments with Sums-of-Squares Programming

Yulin Li¹, Chunxin Zheng², Kai Chen², Yusen Xie², Xindong Tang³,
Michael Yu Wang⁴, *Fellow, IEEE*, and Jun Ma¹

Abstract—In this work, we propose a trajectory optimization approach for robot navigation in cluttered 3D environments. We represent the robot’s geometry as a semialgebraic set defined by polynomial inequalities such that robots with general shapes can be suitably characterized. To address the robot navigation task in obstacle-dense environments, we exploit the free space directly to construct a sequence of free regions, and allocate each waypoint on the trajectory to a specific region. Then, we incorporate a uniform scaling factor for each free region, and formulate a Sums-of-Squares (SOS) optimization problem that renders the containment relationship between the robot and the free space computationally tractable. The SOS optimization problem is further reformulated to a semidefinite program (SDP), and the collision-free constraints are shown to be equivalent to limiting the scaling factor along the entire trajectory. In this context, the robot at a specific configuration is tailored to stay within the free region. Next, to solve the trajectory optimization problem with the proposed safety constraints (which are implicitly dependent on the robot configurations), we derive the analytical solution to the gradient of the minimum scaling factor with respect to the robot configuration. As a result, this seamlessly facilitates the use of gradient-based methods in efficient solving of the trajectory optimization problem. Through a series of simulations and real-world experiments, the proposed trajectory optimization approach is validated in various challenging scenarios, and the results demonstrate its effectiveness in generating collision-free trajectories in dense and intricate environments populated with obstacles.

I. INTRODUCTION

Over the past decade, substantial progress has been made in trajectory optimization for a diverse range of applications in robotics [1]–[3]. At its core, it aims to optimize for a collision-free trajectory that adheres to motion constraints while minimizing a task-specific cost function. Recent accomplishments in numerical optimization have facilitated effective solutions for nonlinear programs with various general constraints and objectives, resulting in improved performance across numerous robotic systems. Nonetheless, the inherent complexity and nonconvexity of the collision-free configuration space still pose significant challenges in effectively

modeling safety constraints, particularly when confronted with intricate and densely populated obstacle layouts. Moreover, accurately formulating collision avoidance constraints often necessitates considering the geometry of the robot and its surrounding environment, which can be difficult to capture explicitly amidst complex robot and obstacle configurations. Consequently, there is a growing demand for advanced trajectory optimization techniques that can effectively address these challenges, substantially facilitating safe and efficient navigation of robots in complex and cluttered environments.

In this paper, we present a trajectory optimization approach that generates collision-free motions for robots with general geometries in intricate and cluttered environments. Specifically, it is achieved by enforcing the containment relationship between the robot and the collision-free workspace over the optimization horizon. We delineate the free space by decomposing it into a series of polytopic regions and constructing a graph to encode their connectivity information. Subsequently, we search for a sequence of free regions with the shortest edge cost that connects the start and goal configurations, based on which each waypoint is allocated to one specific free region. To render the safety condition tractable, we define a uniform scaling factor for the polytopic free region and formulate a Sums-of-Squares (SOS) optimization problem to solve for the minimal scaling factor that certifies the containment relationship between the robot and the scaled free region. It is worth noting that in the formulation of the safety constraints, the geometries of the robots are represented by sets of polynomial inequalities, thereby facilitating the application of this methodology to robots with general shapes. Our proposed SOS optimization problem is further recast as a semidefinite program (SDP). Moreover, the gradient of the scaling factor with respect to the robot configuration is subsequently derived and integrated with gradient-based trajectory optimization algorithm, resulting in an efficient pipeline that propels the trajectory towards the safe and optimal direction with swift and continuous convergence. Lastly, through extensive evaluations in a variety of challenging scenarios, our proposed framework demonstrates its feasibility and efficacy in generating safe and efficient trajectories, and the capability for flexible self-pose adjustment to adapt to complex and cluttered environments is attained.

II. RELATED WORKS

As an indispensable ingredient in trajectory optimization, various approaches have been explored in the literature to

¹Yulin Li and Jun Ma are with the Division of Emerging Interdisciplinary Areas, The Hong Kong University of Science and Technology, Hong Kong SAR, China ylie@connect.ust.hk; jun.ma@ust.hk

²Chunxin Zheng, Kai Chen, and Yusen Xie are with the Robotics and Autonomous Systems Thrust, The Hong Kong University of Science and Technology (Guangzhou), Guangzhou, China czheng739@connect.hkust-gz.edu.cn

³Xindong Tang is with the Department of Mathematics, Hong Kong Baptist University, Hong Kong SAR, China xdtang@hkbu.edu.hk

⁴Michael Yu Wang is with the School of Engineering, Great Bay University, China mywang@gbu.edu.cn

Yulin Li and Chunxin Zheng contributed equally to this work.

formulate collision avoidance constraints in cluttered environments. One category involves exploiting the distance information between robots and obstacles. In [4], distance margins between robot and obstacles are explicitly represented and enforced as state constraints. Analogously, distance functions are used to derive control constraints based on control barrier functions (CBFs), which are then synthesized into the design of safety-critical controllers [5]. However, the distance between two general shapes is inherently implicit, inevitably leading to oversimplified geometries of the robots and obstacles. In [6], [7], equivalent conditions for the implicit CBF constraints are derived by examining the perspective of the dual problem for the optimization problem that solves for the minimum distance between two polytopic sets, resulting in a trajectory optimization problem with nonlinear and nonconvex constraints. Another recent work [8] defines cone representations for several commonly encountered geometry primitives and constructs minimum scaling problems for every pair of collision primitives for collision checking. Gradient information is then extracted and combined with gradient-based solvers for collision-free trajectory generation in the scenario composed of these primitives. Yet, formulating distance constraints for each robot-obstacle pair leads to exponentially increased computational burden in cluttered environments. Additionally, these approaches require prior knowledge of obstacle geometries, which hinders their implementations in environments with intricate obstacle configurations.

Alternatively, a series of works enforce the robot to stay within the obstacle-free workspace [9]–[12]. However, these methods typically assume point or circular robot models due to the intractability of the containment relationship between sets with general geometries. In [13], robots with specific convex geometries are treated as a point, and collision-free trajectory is generated inside the high-dimensional configuration free space, whose decomposition is obtained using the alternating optimization framework proposed in [14]. Although this method achieves high performance for motion planning in obstacle-dense environment, the process of generating such decomposition in high-dimensional configuration space is especially time-consuming, particularly when dealing with obstacles with complex configurations. Subsequently, a safety-critical reactive controller has been proposed that leverages the SOS techniques and moment constraints [15]. This approach filters the nominal twist control, ensuring that the robots with general geometries stay within the locally extracted polytopic free region in the workspace. However, the one-step controller tends to generate conservative and myopic strategies, utilizing only one surrounding free region extracted with current sensor input.

III. PROBLEM STATEMENT

We list relevant notations in Table I for convenience. This work aims to generate collision-free trajectories for robots with specific geometries in obstacle-dense 3D environments. Specifically, we approximately decompose the obstacle-free workspace \mathcal{F} into N overlapping polytopic regions \mathcal{Q}_i with $i = 1, 2, \dots, N$, i.e., $\cup_{i=1:N} \mathcal{Q}_i = \mathcal{Q} \approx \mathcal{F}$. Then, \mathbf{q} is

TABLE I
NOMENCLATURE

Symbols	Descriptions
$\mathbf{q} \in \mathbb{R}^n$	n -dimensional robot configuration
$\mathbf{u} \in \mathbb{R}^m$	m -dimensional control input
$\mathcal{S} \subset \mathbb{R}^3$	3D Euclidean workspace
$\mathcal{W}(\mathcal{o}_i) \subset \mathbb{R}^3$	Space occupied by the i th obstacle
\mathcal{F}	Obstacle-free workspace, i.e., $\mathcal{S} \setminus \cup_{\mathcal{o}_i \in \mathcal{O}} \mathcal{W}(\mathcal{o}_i)$
$\mathcal{W}_{\mathcal{B}}(\mathbf{q}) \subset \mathbb{R}^3$	Space occupied by robot \mathcal{B} at configuration \mathbf{q}
\mathbf{q}_s	Start configuration
\mathbf{q}_g	Goal configuration
$C(\mathcal{Q})$	Geometrical center of a convex shape \mathcal{Q}

considered as a safe configuration if $\mathcal{W}(\mathbf{q}) \subseteq \mathcal{Q}$. Given the above definitions, our goal is to solve for the trajectory $\mathcal{X} = \{\mathbf{q}_0, \mathbf{q}_1, \dots, \mathbf{q}_T\}$ and $U = \{\mathbf{u}_0, \mathbf{u}_1, \dots, \mathbf{u}_{T-1}\}$, which is the solution of the following nonlinear optimization problem over the horizon T :

$$\begin{aligned}
 & \underset{(\mathbf{q}_\tau, \mathbf{u}_\tau) \in \mathbb{R}^n \times \mathbb{R}^m}{\text{minimize}} && \phi_T(\mathbf{q}_T) + \sum_{\tau=0}^{T-1} J_\tau(\mathbf{q}_\tau, \mathbf{u}_\tau) \\
 & \text{subject to} && \mathbf{q}_{\tau+1} = f(\mathbf{q}_\tau, \mathbf{u}_\tau), \\
 & && h_\tau(\mathbf{q}_\tau, \mathbf{u}_\tau) = 0, \\
 & && g_\tau(\mathbf{q}_\tau, \mathbf{u}_\tau) \leq 0, && (1) \\
 & && \tau = 0, 1, \dots, T-1 \\
 & && \mathcal{W}_{\mathcal{B}}(\mathbf{q}_\tau) \subseteq \mathcal{Q}, \\
 & && \tau = 0, 1, \dots, T \\
 & && \mathbf{q}_0 = \mathbf{q}_s.
 \end{aligned}$$

In the above, the subscript τ denotes the corresponding values at that time stamp; $J_\tau(\mathbf{q}_\tau, \mathbf{u}_\tau)$ and ϕ_T represent the intermediate and terminal costs, respectively; $f(\mathbf{q}_\tau, \mathbf{u}_\tau)$ is the discrete dynamic function; $h_\tau(\mathbf{q}_\tau, \mathbf{u}_\tau)$ and $g_\tau(\mathbf{q}_\tau, \mathbf{u}_\tau)$ denote general equality and inequality state-input constraints. Importantly, the constraint $\mathcal{W}_{\mathcal{B}}(\mathbf{q}_\tau) \subseteq \mathcal{Q}$ states that the space occupied by the robot \mathcal{B} at each time stamp is contained in the sets of free regions, thereby ensuring geometry-aware collision-free maneuvers along the whole trajectory. Details of the problem formulation as well as the developed methodology to solve this problem are elaborated in the following section.

IV. METHODOLOGY

A. Waypoints Allocation on Graph of Free Regions

As shown in Fig. 1(a), in an environment with random obstacles, we first generate a family of polytopic free regions at some sampling points using the decomposition algorithm in [9], such that \mathcal{F} can be tightly approximated. Given \mathcal{Q} , we construct an undirected graph $\mathcal{G} := (\mathcal{V}, \mathcal{E})$, where each region \mathcal{Q}_i is assigned to the vertex $v_i \in \mathcal{V}$, and the vertex pair (v_i, v_j) is connected with an edge $e_{i,j} \in \mathcal{E}$ if they have an overlapping area $\mathcal{Q}_{i,j}$. Note that the overlapping area of two of these polytopic free regions, i.e., the intersection of two polytopes, is still a polytope whose representation can be easily obtained by stacking the linear constraints defining the two sets. Edge $e_{i,j}$ is defined as the line segments that connect \mathcal{Q}_i , $\mathcal{Q}_{i,j}$, and \mathcal{Q}_j sequentially through their geometrical centers, and edge cost $\ell_{e_{i,j}}$ is the length of the straight lines.

Subsequently, as shown in Fig. 1(b), we search for a sequence of free regions \mathbb{P}_v^* connecting \mathbf{q}_s and \mathbf{q}_g with the minimal path cost by applying Dijkstra algorithm on \mathcal{G} :

$$\mathbb{P}_v^* = \left\{ \{ \mathbf{q}_s, \mathcal{Q}_0^*, \mathcal{Q}_1^*, \dots, \mathcal{Q}_p^*, \mathbf{q}_g \} \mid \begin{array}{l} \mathcal{W}(\mathbf{q}_s) \subseteq \mathcal{Q}_0^*, \\ \mathcal{W}(\mathbf{q}_g) \subseteq \mathcal{Q}_p^* \end{array} \right\}.$$

We further define two additional edges $e_{s,0}^* = (\mathbf{q}_s, v_0^*)$ and $e_{p,g}^* = (v_p^*, \mathbf{q}_g)$ as the line segments connecting the start position to $C(\mathcal{Q}_0^*)$ and $C(\mathcal{Q}_p^*)$ to the goal position, respectively. Then, the edge sequence concatenating each vertex in \mathbb{P}_v^* can be extracted accordingly:

$$\mathbb{P}_e^* = \{ e_{s,0}^*, e_{0,1}^*, e_{1,2}^*, \dots, e_{p-1,p}^*, e_{p,g}^* \}.$$

To render the safety constraints in (1) computationally tractable, we adopt a heuristic method to enforce the robot to stay inside a designated free region at each time stamp:

$$\mathcal{W}_B(\mathbf{q}_\tau) \subseteq \mathcal{Q}_\tau \quad \forall \tau = 0, 1, \dots, T. \quad (2)$$

Specifically, for a given optimization horizon T , we first discretize the path in \mathbb{P}_e^* by assuming a constant linear velocity to obtain $T + 1$ discrete points, as demonstrated in Fig. 1(c). Then, each waypoint is assigned to the free region containing that point, and the points inside an overlapping area will always be assigned to the latter one according to the order in \mathbb{P}_e^* .

Additionally, as indicated in Fig. 1(d), we generate an extra polytopic region at the geometrical center of an overlapped area $\mathcal{Q}_{i,j}$. This mechanism will be triggered if there exist points on the line segment connecting $C(\mathcal{Q}_i)$ and $C(\mathcal{Q}_j)$ that do not belong to either free region, and the points within the appended region will be reassigned. This intuitive strategy provides the trajectory optimization module with improved quality of free regions, thus facilitating smooth transitions in areas with sharp turns.

Remark 1: The proposed pre-allocating method prevents introducing integer variables in the formulation of optimization problem (1), albeit at the expense of a degree of flexibility in trajectory assignments. However, given that the primary focus of this work is to ensure safety along the trajectory by exploring geometric considerations, and since mixed-integer programming is known to be NP-hard, the pre-allocating method proves to be a more pragmatic and efficient approach.

B. Safety Constraints Formulation with SOS Programming

In this section, we introduce the transformation of the safety condition (2) into an SOS programming problem. Specifically, as illustrated in Fig. 2, we define $\mathcal{Q}_\tau(\alpha)$ as the uniformly scaled polytopic free region with a nonnegative scaling factor α . Then, an optimization problem based on nonnegative polynomials and their SOS approximation is derived, which solves for the minimal scaling factor α such that the containment relationship between the robot and the scaled free region can be theoretically guaranteed. It is worthwhile to note that a solution always exists since the scaled free region can cover the whole Euclidean space \mathbb{R}^3 as α goes to infinity. In this sense, safety condition stated in (2) can be effectively enforced with $\alpha \leq 1$ along the trajectory without loss of generation.

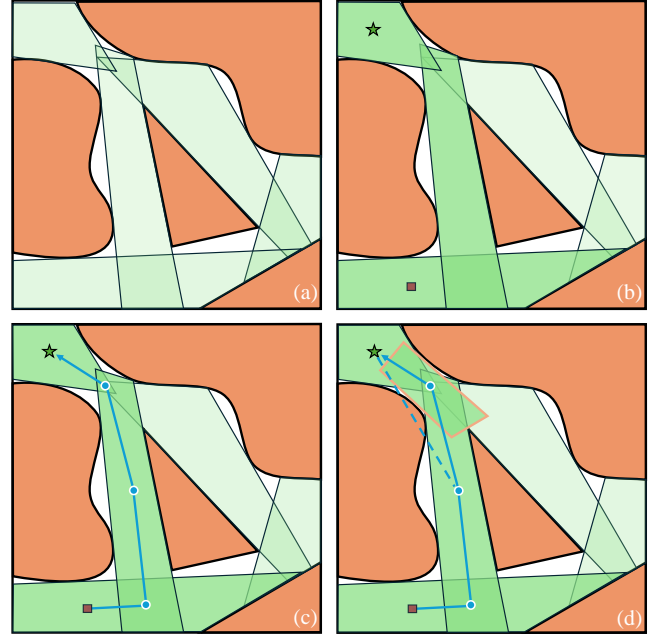


Fig. 1. Illustration of the waypoints allocation process on the constructed graph of free regions \mathcal{G} . (a) The free space \mathcal{F} is decomposed into series of overlapping polytopic regions \mathcal{Q} (the light green polytopic regions). (b) A sequence of the free regions connecting \mathbf{q}_s (the red square) and \mathbf{q}_g (the green star) with minimal path cost is then searched and stored in \mathbb{P}_v^* (emphasized in dark green). (c) Waypoints are allocated to specific free regions along the path connecting the edge between each pair of regions in \mathbb{P}_v^* . (d) Extra regions are generated at the geometrical center of particular overlapped area and the waypoints in each appended region is reallocated for smooth transition.

1) *Set Representation with Polynomial Functions:* We first introduce necessary basis for establishing the containment relationship between two semialgebraic sets defined with polynomial inequalities.

Given a vector $\mathbf{x} = (x_1, x_2, \dots, x_z)$ in \mathbb{R}^z concatenated column-wisely, we denote $\mathbb{R}[\mathbf{x}]$ as the space of all real-coefficient multivariate polynomial functions in \mathbf{x} , and $\mathbb{R}[\mathbf{x}]_d$ is the subset of $\mathbb{R}[\mathbf{x}]$ containing polynomials with degrees no greater than d . We define $\mathbf{x}^\beta := x_1^{\beta_1} x_2^{\beta_2} \dots x_z^{\beta_z}$ a *monomial* in \mathbf{x} for the tuple of nonnegative integers $\beta := (\beta_1, \beta_2, \dots, \beta_z)$. Then, a multivariate polynomial function $f(\mathbf{x}) \in \mathbb{R}[\mathbf{x}]$ can be uniquely expressed with a linear combination of all its monomials:

$$f(\mathbf{x}) = \text{coef}(f)^\top [\mathbf{x}]_{\text{deg}(f)},$$

where $[\mathbf{x}]_d \in \mathbb{R}^{C_{z+d}^d}$ is the vector of all monomials in \mathbf{x} whose degrees are not greater than d ; $\text{coef}(f)$ is the vector of coefficients of f corresponding to each monomial in $[\mathbf{x}]_d$; and $\text{deg}(f)$ denotes the degree of polynomial f . For example, a polynomial $f_0 = 1 + 2x_1 + 3x_2 + 4x_1^2 + 5x_1x_2 + 6x_2^2$ in $\mathbf{x} = (x_1, x_2)$ can be rewritten as $f_0 = (1, 2, 3, 4, 5, 6)^\top (\mathbf{x}^{(0,0)}, \mathbf{x}^{(1,0)}, \mathbf{x}^{(0,1)}, \mathbf{x}^{(2,0)}, \mathbf{x}^{(1,1)}, \mathbf{x}^{(0,2)})$.

A polynomial in \mathbf{x} is said to be an Sum-of-Squares (SOS) if it can be written as the sum of squares of other polynomials. Denote the set of all SOS polynomials as $\Sigma[\mathbf{x}]$, then every SOS polynomial $\sigma \in \Sigma[\mathbf{x}] \cap \mathbb{R}[\mathbf{x}]_{2d}$ can be written in the quadratic form [16]:

$$\sigma = [\mathbf{x}]_d^\top X [\mathbf{x}]_d, \quad (3)$$

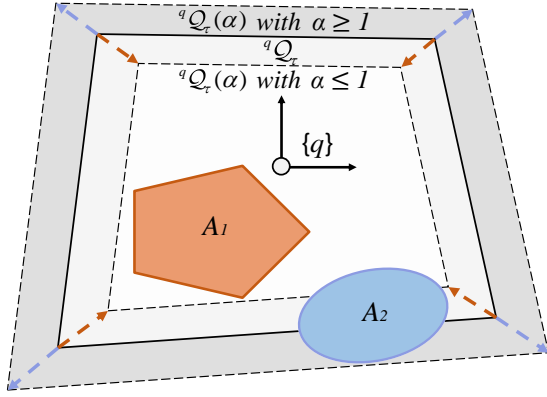


Fig. 2. Geometrical interpretation of the proposed minimum scaling problem. We aim to find the minimum scaling factor α for the polytopic free region ${}^q\mathcal{Q}_\tau$ such that the robots A_1 ($\alpha \leq 1$) and A_2 ($\alpha \geq 1$) are contained in the scaled region.

where $X \in \mathbf{S}_+^{\ell_d}$ is a symmetric positive semidefinite matrix of dimension $\ell_d = C_{z+d}^d = \binom{z+d}{d}$.

For convenience, we will use \mathbf{x} as the 3D coordinates in Euclidean space $\mathbf{x} = (x, y, z)$ in the remaining of this paper to describe the geometrical sets in \mathbb{R}^3 unless otherwise specified. The space occupied by robot \mathcal{B} in its body frame $\{b\}$ is defined with m polynomial inequalities:

$${}^b\mathcal{W}_B := \{\mathbf{x} \in \mathbb{R}^3 : f_1(\mathbf{x}) \geq 0, f_2(\mathbf{x}) \geq 0, \dots, f_m(\mathbf{x}) \geq 0\}.$$

Note that the semialgebraic sets expression can represent robots with the majority of convex shapes and part of non-convex shapes in \mathbb{R}^3 .

For a polytopic free region \mathcal{Q}_τ consisting of r facets, we define it by stacking the linear constraints for each hyperplane into $F \in \mathbb{R}^{r \times 3}$ and $g \in \mathbb{R}^r$ in its own frame q :

$$\begin{aligned} {}^q\mathcal{Q}_\tau &:= \{\mathbf{x} \in \mathbb{R}^3 : g - F^\top \mathbf{x} \geq \mathbf{0}\} \\ &= \{\mathbf{x} \in \mathbb{R}^3 : (g^\top, -F^\top)^\top [\mathbf{x}]_1 \geq \mathbf{0}\}, \end{aligned}$$

where $\mathbf{0}$ denotes the zero vector in \mathbb{R}^r , and $[\mathbf{x}]_1 = (1, x, y, z)$ is the monomial vector of degree 1 in x . The origin of $\{q\}$ is located at $C({}^q\mathcal{Q}_\tau)$ with the axis aligning to the world frame $\{w\}$, as demonstrated in Fig. 2. In this sense, the uniformly scaled free region from $\{q\}$ can be represented as:

$${}^q\mathcal{Q}_\tau(\alpha) := \{\mathbf{x} \in \mathbb{R}^3 : (\alpha g^\top, -F^\top)^\top [\mathbf{x}]_1 \geq \mathbf{0}\},$$

which simply functions as a ratio on the constant term g .

2) *Certified Containment Relationship with Minimum Scaling*: Since the containment relationship in (2) can be stated in any reference frame, we formulate the optimization problem in robot body frame $\{b\}$, in which the set ${}^b\mathcal{W}_B$ will not change with the robot state \mathbf{q} . Denote $R(\mathbf{q}) \in \mathbb{R}^{3 \times 3}$ and $p(\mathbf{q}) \in \mathbb{R}^3$ the rotation matrix and translation vector representing the configuration of robot body frame $\{b\}$ in $\{q\}$, the scaled free region can be represented in $\{b\}$ as:

$${}^b\mathcal{Q}_\tau(\alpha, \mathbf{q}) := \{\mathbf{x} \in \mathbb{R}^3 : ((\alpha g - Fp)^\top, -(FR)^\top)^\top [\mathbf{x}]_1 \geq \mathbf{0}\},$$

where R and p depend on the robot state \mathbf{q} . In this subsection, we construct the optimization problem solving for the mini-

mal scaling factor α that certifies the following containment relationship in robot body frame:

$${}^b\mathcal{W}_B \subseteq {}^b\mathcal{Q}_\tau(\alpha, \mathbf{q}). \quad (4)$$

Let $\mathcal{P}({}^b\mathcal{W}_B)$ be the set of all the nonnegative polynomials on ${}^b\mathcal{W}_B$, which is defined as:

$$\mathcal{P}({}^b\mathcal{W}_B) = \{f \in \mathbb{R}[\mathbf{x}] : f(\mathbf{x}) \geq 0 \forall \mathbf{x} \in {}^b\mathcal{W}_B\}.$$

Denote $f^{\mathcal{Q}_\tau}$ the vector of the r defining polynomials in ${}^b\mathcal{Q}_\tau(\alpha, \mathbf{q})$. The minimal scaling problem certifying the set containment relationship (4) is then re-stated in terms of the nonnegative polynomials cone on ${}^b\mathcal{W}_B$:

$$\begin{aligned} \min_{\alpha} \quad & \alpha \\ \text{s.t.} \quad & f_i^{\mathcal{Q}_\tau} \in \mathcal{P}({}^b\mathcal{W}_B) \\ & \forall i = 1, 2, \dots, r \\ & \alpha \geq 0. \end{aligned} \quad (5)$$

Here, $f_i^{\mathcal{Q}_\tau}$ represents the i th row of the polynomial vector $f^{\mathcal{Q}_\tau}$, which corresponds to the linear constraint defining the i th facet of the polytope. In the context of polynomial optimization, **Putinar Positivstellensatz** [17] provides us the theoretical guarantee to approximate $\mathcal{P}({}^b\mathcal{W}_B)$ with its **quadratic module** (Qmod) such that (5) can be described explicitly. The $2k$ truncation of Qmod for the defining polynomials f in ${}^b\mathcal{W}_B$ can be written as:

$$\text{Qmod}[f]_{2k} := \{\sigma_0 + f_1\sigma_1 + \dots + f_m\sigma_m : \sigma_0, \dots, \sigma_m \in \Sigma[\mathbf{x}]\},$$

with $\sigma_0 \in \Sigma[\mathbf{x}] \cap \mathbb{R}[\mathbf{x}]_{2k}$ and $\sigma_i \in \Sigma[\mathbf{x}] \cap \mathbb{R}[\mathbf{x}]_{2[k - \deg(f_i)/2]}$ for all $i = 1, 2, \dots, m$.

Consider a nonnegative relaxation order k with $k \geq \lceil \max\{\deg(f^{\mathcal{Q}_\tau}), \deg(f_1)/2, \deg(f_2)/2, \dots, \deg(f_m)/2\} \rceil$, the k th SOS relaxation of (5) is formulated as:

$$\min_{\alpha, \sigma_{i,j}} \quad \alpha \quad (6)$$

$$\text{s.t.} \quad f_i^{\mathcal{Q}_\tau} = \sigma_{i,0} + \sum_{j=1}^m f_j \cdot \sigma_{i,j}, \quad (6a)$$

$$\forall i = 1, 2, \dots, r$$

$$\sigma_{i,0} \in \Sigma[\mathbf{x}] \cap \mathbb{R}[\mathbf{x}]_{2k}, \quad (6b)$$

$$\sigma_{i,j} \in \Sigma[\mathbf{x}] \cap \mathbb{R}[\mathbf{x}]_{2[k - \deg(f_j)/2]}, \quad (6c)$$

$$\forall i = 1, 2, \dots, r, \forall j = 1, 2, \dots, m$$

$$\alpha \geq 0. \quad (6d)$$

Given a robot state \mathbf{q} , specifically the fixed $R(\mathbf{q})$ and $p(\mathbf{q})$, the formulated problem (6) is a standard SOS program since the decision variable α is linear in the coefficients of certain monomials. To facilitate the employment of conic programming solvers and the further derivation of gradient, we transform

(6) into an SDP by expressing the SOS polynomials into the quadratic form as in (3):

$$\min_{\alpha, X_{i,j}} \alpha \quad (7)$$

$$\text{s.t. } \text{coef}(f_i^{\mathcal{Q}_\tau})_l - \sum_{j=0}^m \langle A_{(i,l),j}, X_{i,j} \rangle = 0, \quad (7a)$$

$$\forall i = 1, 2, \dots, r, \forall l = 1, 2, \dots, \ell$$

$$X_{i,0} \in \mathbf{S}_+^{\ell_0}, \ell_0 = \begin{pmatrix} z+k \\ k \end{pmatrix}, \quad (7b)$$

$$X_{i,j} \in \mathbf{S}_+^{\ell_j}, \ell_j = \begin{pmatrix} z + \lfloor k - \deg(f_j)/2 \rfloor \\ \lfloor k - \deg(f_j)/2 \rfloor \end{pmatrix}, \quad (7c)$$

$$\forall i = 1, 2, \dots, r, \forall j = 1, 2, \dots, m$$

$$\alpha \geq 0. \quad (7d)$$

In (7), $\langle \cdot, \cdot \rangle$ represents the inner product between two matrices, and z is the dimension of the intermediates \mathbf{x} . Note that (7a) is obtained by enforcing equality constraints on the coefficients corresponding to all ℓ monomials involved in (6a).

Remark 2: Since we have designated each waypoint on the trajectory \mathcal{X} to a specific free region in Sec. IV-A, and considering that the set representation ${}^b\mathcal{W}_B$ will not change with different robot configurations, it is possible to pre-compute all the matrix coefficients A , and therefore it greatly speeds up the online solving process.

C. Collision-Free Trajectory Optimization with Implicit Safety Constraints

With the geometrical interpretation of the containment relationship in (2), we define a uniformly scaling factor α_τ for each waypoint \mathbf{q}_τ in \mathcal{X} , and reformulate the collision-free trajectory optimization problem (1) as:

$$\begin{aligned} & \underset{(\mathbf{q}_\tau, \mathbf{u}_\tau) \in \mathbb{R}^n \times \mathbb{R}^m}{\text{minimize}} && \phi_T(\mathbf{q}_T) + \sum_{\tau=0}^{T-1} J_\tau(\mathbf{q}_\tau, \mathbf{u}_\tau) \\ & \text{subject to} && \mathbf{q}_{\tau+1} = f(\mathbf{q}_\tau, \mathbf{u}_\tau), \\ & && h_\tau(\mathbf{q}_\tau, \mathbf{u}_\tau) = 0, \\ & && g_\tau(\mathbf{q}_\tau, \mathbf{u}_\tau) \leq 0, \\ & && \tau = 0, 1, \dots, T-1 \\ & && \alpha_\tau(\mathbf{q}_\tau) \leq 1, \\ & && \tau = 0, 1, \dots, T \\ & && \mathbf{q}_0 = \mathbf{q}_s. \end{aligned} \quad (8)$$

In (8), motion safety considering geometry of the robot is ensured by enforcing α_τ to be no greater than one over the entire optimization horizon, where $\alpha_\tau(\mathbf{q}_\tau)$ is the optimum of the proposed minimum scaling problem (5), which is implicitly dependent on the robot configuration \mathbf{q} at time stamp τ . In this section, to deal with the implicit safety constraints, we further derive the gradient of the scaling factor with respect to the robot configuration $\partial\alpha/\partial\mathbf{q} \in \mathbb{R}^n$ analytically. This facilitates the seamless incorporation of the proposed optimization problem (7) into gradient-based trajectory optimization algorithms, thereby enabling the effective solving of the nonlinear program (8) with the proposed implicit safety constraints.

In (7), α is simply the objective function, and in this case, $\partial\alpha/\partial\mathbf{q}$ can be effectively extracted by calculating the partial derivative of the Lagrangian function \mathcal{L} with respect the robot configuration \mathbf{q} at the primal-dual optimum of the SDP (7). Furthermore, since the rotation matrix $R(\mathbf{q})$ and translation vector $p(\mathbf{q})$ only appear in the coefficients of $f^\mathcal{Q}$, it is only necessary to consider the Lagrange multipliers corresponding to the constraints in (7a) to compute the gradient. In this sense, the gradient vector can be represented as:

$$\frac{\partial\alpha}{\partial\mathbf{q}} = \frac{\partial\mathcal{L}}{\partial\mathbf{q}} = \sum_{i,l} \lambda_{i,l} \frac{\partial(\text{coef}(f_i^{\mathcal{Q}_\tau})_l)}{\partial\mathbf{q}}, \quad (9)$$

where $\lambda_{i,l}$ is the dual variable for each constraint in (7a). It is worthwhile to highlight that, with the analytical solution in (9), we can efficiently determine the gradient value after solving (7) to its optimum.

Remark 3: Under generic optimality conditions, optimal solutions of (7) and (5) are identical for all k that is sufficiently large [18]. This situation can be further improved if all the polynomial functions involved are SOS-convex [16], under which condition the SOS relaxation at the lowest order is exact.

Subsequently, we employ the gradient-based algorithm Augmented Lagrangian Iterative Linear Quadratic Regulator (AL-iLQR) proposed in [19]. In this approach, the constraints can be augmented into the objective function and solved iteratively using the iLQR algorithm. Specifically, we calculate the value of α as well as its gradient with respect to the robot configuration \mathbf{q} based on the trajectory output from each round of forward pass of AL-iLQR. We then integrate this information in the execution of the backward pass of AL-iLQR to calculate the perturbed action, enforcing the robot to stay inside the free regions \mathcal{Q} . Notably, the process of solving the proposed SDP and extracting gradients along the trajectory is significantly accelerated through precomputation and parallelization.

To this end, the proposed collision-free trajectory optimization method considering specific robot geometries is summarized in Algorithm 1.

V. RESULTS

In this section, we conduct a thorough evaluation of our proposed trajectory optimization approach through simulations and real-world experiments. We deploy the algorithm on an Intel i5-13400F processor, and the proposed SDP in (7) is implemented and solved parallelly using MOSEK [20] with precomputation of the pertinent parameters. In simulations, we initially validate our algorithm on robots modeled with various geometries represented as semialgebraic sets, including a polytope, a cylinder, an ellipsoid, and an elliptical cone. We analyze typical scenarios where waypoints fail to converge into the free regions and discuss how we address these issues with specific ingredients. Subsequently, we demonstrate the efficacy and robustness of our algorithm for collision-free trajectory optimization in three challenging maze scenarios with different degrees of complexity. Finally, we apply the trajectory optimization pipeline on the real robot platform

Algorithm 1: Collision-Free Trajectory Optimization with SOS Programming

Input: \mathcal{Q} , \mathbf{q}_s , \mathbf{q}_g , T , $ctol$, and ${}^b\mathcal{W}_B$
Output: \mathcal{X}^* and U^*

```

1 Function WaypointsAllocation( $\mathcal{Q}$ ,  $\mathbf{q}_s$ ,  $\mathbf{q}_g$ ,  $T$ ):
2    $\mathcal{V} \leftarrow$  Assign each region  $\mathcal{Q}_i$  in  $\mathcal{Q}$  to a vertex  $v_i$ ;
3    $\mathcal{E} \leftarrow$  Connect  $(v_i, v_j)$  in  $\mathcal{V}$  if they are overlapped;
4    $\mathbb{P}_v^* \leftarrow$  Search for free regions sequence connecting  $\mathbf{q}_s$ 
   and  $\mathbf{q}_g$  with shortest path length;
5    $\mathbb{P}_e^* \leftarrow$  Extract the edge sequence concatenating vertices
   in  $\mathbb{P}_v^*$ ;
6   Index  $\leftarrow$  Assign each waypoint to a free region with
    $\mathbb{P}_e^*$  and the optimization horizon  $T$ ;
7   Index  $\leftarrow$  Add additional regions and reassign
   waypoints;
8   return Index
9 Initialization:
10  $\mathcal{X}^* \leftarrow \mathcal{X}_0$  and  $U^* \leftarrow U_0$ ;
11  $ctol \leftarrow$  Tolerance of constraints violation in AL-iLQR;
12  $c \leftarrow$  Constraints violation of current trajectory;
13 Index  $\leftarrow$  WaypointsAllocation( $\mathcal{Q}$ ,  $\mathbf{q}_s$ ,  $\mathbf{q}_g$ ,  $T$ );
14 while  $c \geq ctol$  do
15   parfor  $\mathbf{q}_\tau \in \mathcal{X}^*$  :
16      $\alpha_\tau, \partial\alpha_\tau/\partial\mathbf{q} \leftarrow$  Solve (7) and calculate gradients
     from (9) with Index;
17   end
18    $\delta u \leftarrow$  ALiLQR-BACKWARDPASS( $\mathcal{X}^*$ ,  $U^*$ ,  $\alpha$ ,  $\frac{\partial\alpha}{\partial\mathbf{q}}$ );
19    $\mathcal{X}^*$ ,  $U^*$ ,  $c \leftarrow$  ALiLQR-FORWARDPASS( $\mathcal{X}^*$ ,  $U^*$ ,  $\delta u$ )
20 end

```

Unitree Go1, which showcases the adaptability and practicality of our method for safely navigating through a cluttered indoor environment. The entire process is implemented on an intel NUC11 with i5-7260U processor.

A. Simulations

1) *Algorithm Validation for Various Robot Geometries:* In this scenario, we validate the effectiveness of our proposed safety constraints on robots with different geometries. We initialize the trajectories at random configurations and command the robots to stop within the safe region by enforcing the terminal safety constraint, i.e., $\alpha_T(\mathbf{q}_T) \leq 1$. As shown in Fig. 3, trajectories for robots with all geometries have successfully been “attracted” into the designated region with the help of the proposed minimal scaling problem (7) as well as its gradients information (9).

The semialgebraic set descriptions for each involved robot geometry are listed in Table II, which is defined in their body frames as shown in Fig. 3. Note that the polynomial functions defining the geometries are all SOS-convex. We achieve 12 ± 5 ms in average for solving the proposed SDP at the minimum relaxation order since the polynomial functions defining the geometries are all SOS-convex, and the time spent on formulating the SDP and calculating the gradient can be neglected as the explicit expressions have been pre-computed.

Several ingredients are added in our method to ensure the convergence of (8) with our derived safety constraints. For the SDP (7), the Lagrange multiplier $\lambda_{i,l}$ is zero unless the corresponding constraint is active at the primal-dual optimum,

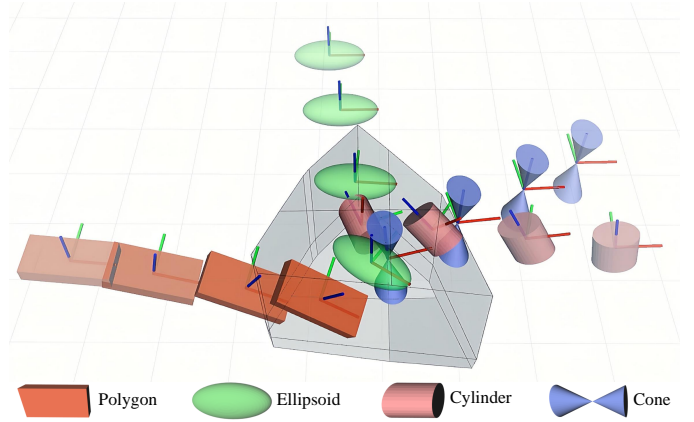


Fig. 3. Visualization of the optimized trajectories for robots with different geometries. The robots are commanded to move into the free region (shown in grey) from random start configurations by enforcing our derived safety constraints at the terminal time stamp.

TABLE II
GEOMETRY DESCRIPTIONS OF THE SETS \mathcal{W}_B FOR DIFFERENT GEOMETRIES

Geometries	\mathcal{W}_B
Polytope	$\{\mathbf{x} = (x, y, z) : \mathbf{A}\mathbf{x} \leq \mathbf{b}\}$
Ellipsoid	$\{\mathbf{x} = (x, y, z) : \frac{x^2}{a^2} + \frac{y^2}{b^2} + \frac{z^2}{c^2} \leq 1\}$
Elliptical Cylinder	$\{\mathbf{x} = (x, y, z) : \frac{x^2}{a^2} + \frac{y^2}{b^2} \leq 1, z \geq -\frac{h}{2}, z \leq \frac{h}{2}\}$
Elliptical Cone	$\{\mathbf{x} = (x, y, z) : \frac{x^2}{a^2} + \frac{y^2}{b^2} \leq \frac{z^2}{c^2}, z \geq -\frac{h}{2}, z \leq \frac{h}{2}\}$

as elaborated in the complementary slackness of KKT optimality conditions [21]. Typically, as indicated in Fig. 2, only the constraints corresponding to the facet that restricts further decrease of α is active at the optimum of the proposed minimum scaling problem. Thus, we use the information of the most difficult-to-satisfy facet for the gradients computation (9) to push the robot towards a safer configuration. This mechanism fails to efficiently utilize all the information from the violated faces to collectively push the robot into the safe region, and could potentially lead to unexpected local optima during line search process, due to the discontinuity from facet switching. To address this problem, we extract the gradients of all violated facets and synthesize them into a more representative gradient by continuously relaxing the constraints of the corresponding facets in (7a) and re-solving the SDP. Another observation from the results is that the gradient scale for translational motion is larger than that for rotational motion. This results in negligible changes in the rotation angle after line search if both rotational and translational motions are searched simultaneously, even if a better trajectory exists with larger changes in the rotation angle. In this sense, we adopt a two-layer line search scheme for translation and rotation separately to avoid trapping into the local optimum and ensure continuous convergence.

2) *Traversing in Mazes:* To evaluate the performance of our proposed trajectory optimization framework in challenging scenarios, we have crafted three distinct mazes of varying dimensions and degrees of complexity, namely the large, medium, and small mazes, respectively, as shown in Fig. 4(a)-

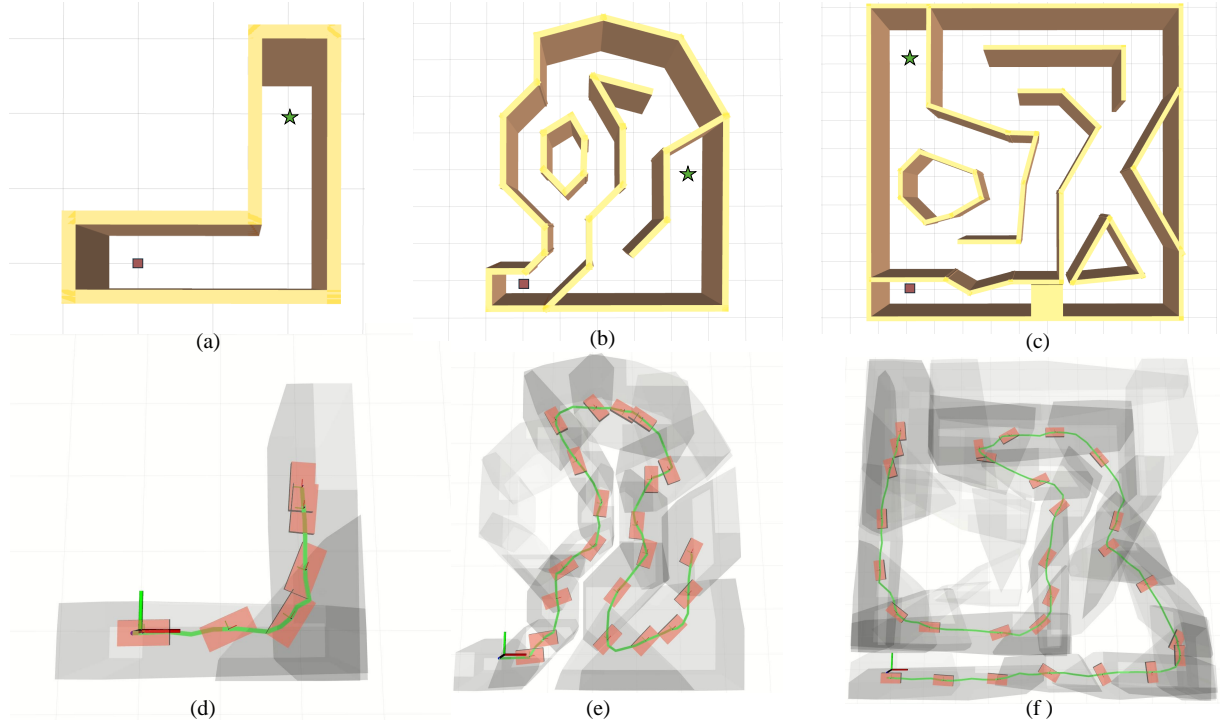


Fig. 4. Performance of our proposed trajectory optimization framework in maze traversing tasks. (a-c) Three maze scenarios with different degrees of complexity. The start and goal positions are denoted by red and green nodes, respectively. (d-f) Visualization of the collision-free trajectories generated by the proposed method in all the three maze scenarios with key frames highlighted.

4(c). To demonstrate the significance of the two proposed ingredients, we conduct two sets of ablation experiments: one with our method excluding gradient synthesis (Ours w/o GS), and the other with our method excluding the two-layer line search (Ours w/o TLS). We record the optimization horizons in the three maze scenarios, as well as the number of iterations before the AL-iLQR cost ceases to decrease for the three different experimental settings, and the final count of waypoints outside the safe region. Observed from Table III, it is evident that as the complexity of the scene increases, the absence of these two ingredients makes it more susceptible to local optimum, which leads to an inability to further reduce the cost associated with safety constraints, thereby resulting in unsafe situations. Remarkably, our method successfully optimizes collision-free trajectories in all the three scenarios with the smallest number of iterations. As depicted in the Fig. 4(d)-4(f), our optimized trajectories enable the robot to navigate through diverse complex maze environments by adopting different degrees of posture adjustments based on its shape, thereby demonstrating the effectiveness of our collision-free trajectory optimization method.

B. Real-World Experiment

In this section, we demonstrate the practicality and robustness of our proposed method by deploying it on a real robot platform Unitree Go1. In the experiment, the quadruped is commanded to traverse through a cluttered indoor area of $2\text{ m} \times 6\text{ m}$ with several randomly placed obstacles and a hole to simulate the height-constrained situation.

TABLE III
COMPARISONS BETWEEN OUR METHOD WITH OR WITHOUT TWO KEY INGREDIENTS IN MAZE SCENARIOS

Maze	Waypoints	Method	Iterations	Collisions
Large	143	Ours w/o GS	15	9
		Ours w/o TLS	18	13
		Ours	16	0
Medium	70	Ours w/o GS	17	7
		Ours w/o TLS	13	9
		Ours	11	0
Small	16	Ours w/o GS	6	2
		Ours w/o TLS	7	0
		Ours	5	0

We use the onboard Robosense 16-line spinning Lidar to perceive point cloud data for off-line space decomposition and real-time align-based localization. We incorporate additional physical constraints of the quadruped in the trajectory optimization process and implement the kinematic feedforward and feedback controllers introduced in [22] for trajectory tracking. The computed body twist commands are subsequently fed into the embedded speed controller to actuate each joint on the robot. The robot, along with the onboard sensor, is approximated as a polytope. The proposed optimization problem (7) is solved in around $15 \pm 3\text{ ms}$. As depicted in Fig. 5, the quadruped adjusts its pose to adapt to the obstacle configurations, and due to the tightly fitted robot geometry,

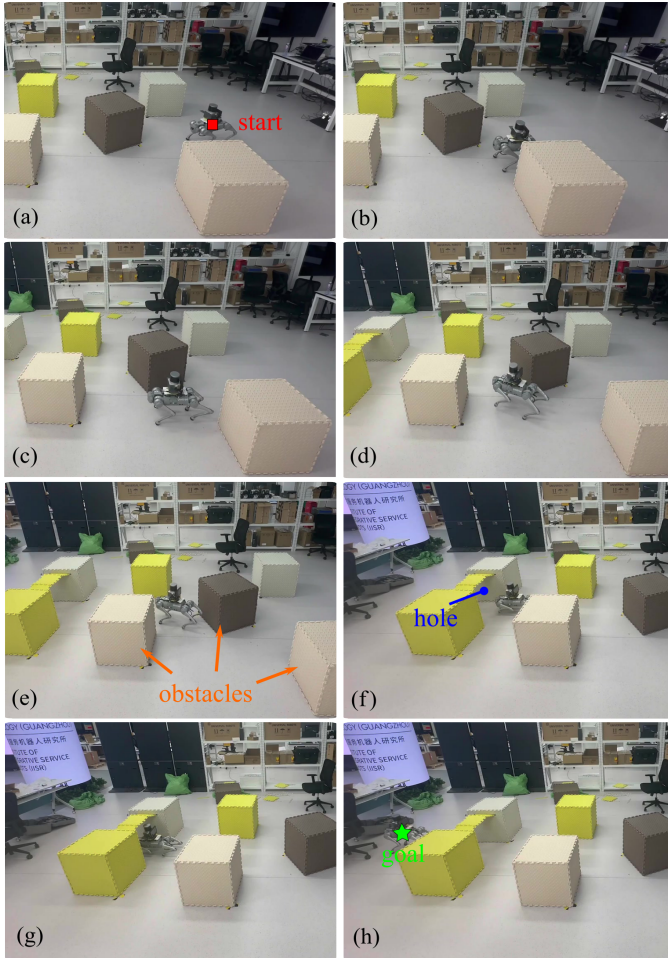


Fig. 5. Snapshots of real-world experiments with our proposed method. The quadruped is commanded to traverse through the cluttered indoor environment with randomly placed obstacles and a hole.

the quadruped lowers its pose to successfully traverse the height-constrained hole in a non-conservative manner (shown in Fig. 5(g)-5(i)). Overall, our proposed framework exhibits remarkable capacity for generating safe and flexible maneuvers in the presence of complex obstacle configurations.

VI. CONCLUSION

This paper introduces a novel framework for optimizing collision-free trajectories to navigate robots safely in cluttered environments. Our approach decomposes the free space into overlapping polytopic regions and formulates an SOS optimization problem to determine the minimum scaling factor for each region, such that the robot with specific geometry is contained within the scaled free region. We enforce the geometry-aware safety constraints by restricting that the scaling factor to be less than 1 along the entire trajectory. Importantly, the SOS programming is transformed into a convex SDP, which enables efficient computation of the solution and gradient information that are then integrated with AL-iLQR to generate effective and flexible collision-free trajectories. We extensively evaluate our proposed algorithm in both simulations and real-world experiments, and the results demonstrate that our method is

capable of generating effective and flexible obstacle avoidance maneuvers when navigating the robot through challenging environments.

REFERENCES

- [1] W. Xu, Q. Wang, and J. M. Dolan, "Autonomous vehicle motion planning via recurrent spline optimization," in *2021 IEEE International Conference on Robotics and Automation*, 2021, pp. 7730–7736.
- [2] J. P. Sleiman, F. Farshidian, and M. Hutter, "Constraint handling in continuous-time DDP-based model predictive control," in *2021 IEEE International Conference on Robotics and Automation*, 2021, pp. 8209–8215.
- [3] A. W. Winkler, C. D. Bellicoso, M. Hutter, and J. Buchli, "Gait and trajectory optimization for legged systems through phase-based end-effector parameterization," *IEEE Robotics and Automation Letters*, vol. 3, no. 3, pp. 1560–1567, 2018.
- [4] Z. Li, J. Zeng, S. Chen, and K. Sreenath, "Autonomous navigation of underactuated bipedal robots in height-constrained environments," *The International Journal of Robotics Research*, vol. 42, no. 8, pp. 565–585, 2023.
- [5] A. D. Ames, S. Coogan, M. Egerstedt, G. Notomista, K. Sreenath, and P. Tabuada, "Control barrier functions: Theory and applications," in *2019 18th European Control Conference*, 2019, pp. 3420–3431.
- [6] A. Thirugnanam, J. Zeng, and K. Sreenath, "Safety-critical control and planning for obstacle avoidance between polytopes with control barrier functions," in *2022 International Conference on Robotics and Automation (ICRA)*, 2022, pp. 286–292.
- [7] Q. Liao, Z. Li, A. Thirugnanam, J. Zeng, and K. Sreenath, "Walking in narrow spaces: Safety-critical locomotion control for quadrupedal robots with duality-based optimization," in *2023 IEEE International Conference on Intelligent Robots and Systems*, 2023, pp. 2723–2730.
- [8] K. Tracy, T. A. Howell, and Z. Manchester, "Differentiable collision detection for a set of convex primitives," in *2023 IEEE International Conference on Robotics and Automation*, 2023, pp. 3663–3670.
- [9] S. Liu, M. Watterson, K. Mohta, K. Sun, S. Bhattacharya, C. J. Taylor, and V. Kumar, "Planning dynamically feasible trajectories for quadrotors using safe flight corridors in 3-D complex environments," *IEEE Robotics and Automation Letters*, vol. 2, no. 3, pp. 1688–1695, 2017.
- [10] Y. Ren, F. Zhu, W. Liu, Z. Wang, Y. Lin, F. Gao, and F. Zhang, "Bubble planner: Planning high-speed smooth quadrotor trajectories using receding corridors," in *2022 IEEE/RSJ International Conference on Intelligent Robots and Systems*, 2022, pp. 6332–6339.
- [11] K. Chen, H. Liu, Y. Li, J. Duan, L. Zhu, and J. Ma, "Robot navigation in unknown and cluttered workspace with dynamical system modulation in starshaped roadmap," *arXiv preprint arXiv:2403.11484*, 2024.
- [12] R. Deits and R. Tedrake, "Efficient mixed-integer planning for UAVs in cluttered environments," in *2015 IEEE International Conference on Robotics and Automation*, 2015, pp. 42–49.
- [13] T. Marcucci, M. Petersen, D. von Wrangel, and R. Tedrake, "Motion planning around obstacles with convex optimization," *Science Robotics*, vol. 8, no. 84, p. eadf7843, 2023.
- [14] H. Dai, A. Amice, P. Werner, A. Zhang, and R. Tedrake, "Certified polyhedral decompositions of collision-free configuration space," *The International Journal of Robotics Research*, vol. 0, no. 0, 2023.
- [15] Y. Li, X. Tang, K. Chen, C. Zheng, H. Liu, and J. Ma, "Geometry-aware safety-critical local reactive controller for robot navigation in unknown and cluttered environments," *IEEE Robotics and Automation Letters*, vol. 9, no. 4, pp. 3419–3426, 2024.
- [16] J. Nie, *Moment and Polynomial Optimization*. Philadelphia, PA: Society for Industrial and Applied Mathematics, 2023.
- [17] M. Putinar, "Positive polynomials on compact semi-algebraic sets," *Indiana University Mathematics Journal*, vol. 42, no. 3, pp. 969–984, 1993.
- [18] J. Nie, "Optimality conditions and finite convergence of Lasserre's hierarchy," *Mathematical Programming*, vol. 146, pp. 97–121, 2014.
- [19] T. A. Howell, B. E. Jackson, and Z. Manchester, "ALTRO: A fast solver for constrained trajectory optimization," in *2019 IEEE/RSJ International Conference on Intelligent Robots and Systems*, 2019, pp. 7674–7679.
- [20] M. ApS, *The MOSEK Optimization Toolbox for MATLAB Manual. Version 10.0.*, 2022. [Online]. Available: <http://docs.mosek.com/10.0/toolbox/index.html>
- [21] S. Boyd and L. Vandenberghe, *Convex Optimization*. Cambridge, UK: Cambridge University Press, 2004.
- [22] K. M. Lynch and F. C. Park, *Modern Robotics*. Cambridge, UK: Cambridge University Press, 2017.